

# Oxygen Reduction Reaction Promotes $\text{Li}^+$ Desorption from Cathode Surface in $\text{Li-O}_2$ Batteries

Marta Haro,\* Nuria Vicente, and Germà Garcia-Belmonte\*

**Li-O<sub>2</sub> batteries are claimed to be one of the future energy storage technologies. Great number of scientific and technological challenges should be solved first to transform Li-O<sub>2</sub> battery from a promise to real practical devices. Proposed mechanisms for oxygen reduction assume a reservoir of solved Li<sup>+</sup> ions in the electrolyte. However, the role that adsorbed Li<sup>+</sup> on the electrode surface might have on the overall oxygen reduction reaction (ORR) has not deserved much attention. Adsorbed Li<sup>+</sup> consumption is monitored here using impedance measurements from extended electrochemical double layer capacitance, which depends on the carbon matrix surface area. The presence of O<sub>2</sub> drastically reduces the amount of adsorbed Li<sup>+</sup>, signaling the kinetic competition between Li<sup>+</sup> surface adsorption and its consumption, only for potentials corresponding to the oxygen reduction reaction. Noticeably double layer capacitance remains unaltered after cycling. This fact suggests that the ORR products (Li<sub>2</sub>O<sub>2</sub> and Li<sub>2</sub>CO<sub>3</sub>) are not covering the internal electrode surface, but deposited on the outer electrode-contact interface, hindering thereby the subsequent reaction. Current results show new insights into the discharge mechanism of Li-O<sub>2</sub> batteries and reveal the evidence of Li<sup>+</sup> desorption from the C surface when the ORR starts.**

## 1. Introduction

In an increasingly energy-dependent society, the need for renewable energy sources together to its storage is paramount to maintain current society paradigm in a sustainable way with the environment. Albeit Li-ion batteries (LIBs) have invaded the electronic market, their energy densities are usually limited below 250 Wh kg<sup>-1</sup>.<sup>[1]</sup> This limitation is mainly originated by the mechanisms through which the chemical energy is stored in the present commercial LIBs that is based on the reversible reaction of the electrode materials with Li<sup>+</sup> ions by means of intercalation processes. Therefore, approaches based on new chemistry are necessary to increase the energy density in batteries, such as Li-S and Li-O<sub>2</sub>, which can provide more than 1000 Wh kg<sup>-1</sup>.<sup>[2]</sup> In particular, Li-O<sub>2</sub> batteries have received a great deal of attention as they can deliver the highest energy density among any other type of batteries. Li<sup>+</sup> ions and O<sub>2</sub> directly react with each other in the absence of any heavy

transition metals or crystal framework.<sup>[3]</sup> Nevertheless, Li-O<sub>2</sub> battery technology is in its infancy and many fundamental issues are needed to be addressed before their practical application.

The chemical energy storage in Li-O<sub>2</sub> batteries is based on the oxygen reduction reaction (ORR) during discharge and oxygen evolution reaction (OER) in the charge,  $2 \text{Li}^+ + \text{O}_2 + 2 \text{e}^- \leftrightarrow \text{Li}_2\text{O}_2$  ( $E^\circ = 2.96 \text{ V}$ , with theoretical specific energy of 3500 Wh kg<sup>-1</sup>). To date, Li<sub>2</sub>O<sub>2</sub> has been identified as the main discharge product by different techniques such as Raman spectroscopy<sup>[4]</sup> and atomic force microscopy (AFM).<sup>[5]</sup> Li<sub>2</sub>O<sub>2</sub> is electronically insulating, very oxidative and insoluble, precipitating onto the electrode what causes the increase of the necessary potential for OER and the oxidation of the carbon electrode and/or electrolyte giving Li<sub>2</sub>CO<sub>3</sub>,<sup>[6]</sup> and as a consequence the decrease of the cycleability of the Li-O<sub>2</sub> battery. Also, some authors note that the insulating nature

of Li<sub>2</sub>O<sub>2</sub> avoids its possible reduction to Li<sub>2</sub>O, in this situation, Li-O<sub>2</sub> batteries would provide energy densities as high as 5200 Wh kg<sup>-1</sup>.<sup>[7]</sup>

It is then relevant that to fully exploit the capacity of Li-O<sub>2</sub> batteries, the thermodynamic and kinetic mechanisms that govern and limit their functioning must be understood. From the pioneering studies of Abraham and co-workers<sup>[8]</sup> on the ORR to date, the oxygen reduction reaction has been widely analyzed in Li-O<sub>2</sub> batteries,<sup>[9]</sup> and several models have been proposed, which have been recently unified by Bruce and co-workers.<sup>[10]</sup> Generally, the adsorption of O<sub>2</sub> molecules onto the cathode with one electron interchanged with the electrode is considered as the first step ( $\text{O}_2 + \text{e}^- \leftrightarrow \text{O}_2^-$ ,  $E^\circ = 2.71 \text{ V}$ ). This adsorbed O<sub>2</sub><sup>-</sup> reacts with Li<sup>+</sup> ions to produce LiO<sub>2</sub> adsorbed or as solid dissolved in the electrolyte. Depending on the solvent nature and the chemisorption strength with the cathode different mechanisms have been proposed for the reaction of the adsorbed LiO<sub>2</sub> with Li<sup>+</sup> ions until Li<sub>2</sub>O<sub>2</sub> is reached as final product. In all these studies, the ORR starts with the reduction of oxygen in the context of free electrode surface and solved Li<sup>+</sup> ions in the electrolyte. However, the role that adsorbed Li<sup>+</sup> ions on the electrode surface might have on the overall ORR has not deserved much attention. This last contribution was pointed out by Qu and co-workers,<sup>[11]</sup> although no experimental evidence was provided. The monitoring for the first time of the desorption process of

Dr. M. Haro, N. Vicente, Prof. G. Garcia-Belmonte  
Institute of Advanced Materials (INAM)  
Universitat Jaume I  
ES-12071, Castelló, Spain  
E-mail: mharo@uji.es; garciag@uji.es



DOI: 10.1002/admi.201500369

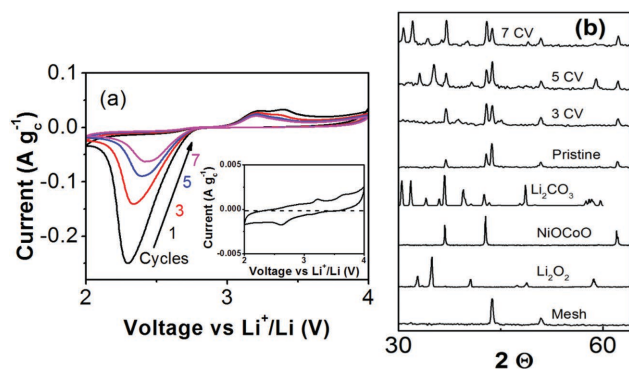


**Figure 1.** a) CV of SP@30%NiOCoO in the presence of O<sub>2</sub> along different number of cycles and in the absence of O<sub>2</sub> (inset). Scan rate: 0.1 mV s<sup>-1</sup>. b) XRD patterns of air cathode after being cycled (3, 5 and 7 cycles). The patterns of the pristine mesh, Li<sub>2</sub>O<sub>2</sub>, NiOCoO, and Li<sub>2</sub>CO<sub>3</sub> are also shown.

Li<sup>+</sup> ions induced by ORR provides here revealing insights on the cathode surface processes in Li-O<sub>2</sub> batteries.

In this article, Li-O<sub>2</sub> discharge process in different cathodes has been monitored by electrochemical impedance spectroscopy (EIS). This technique has been recently used suggesting that the overpotential during discharge is caused by internal resistance, and is dominated by the charge transport through the deposited Li<sub>2</sub>O<sub>2</sub> at the end of discharge.<sup>[6,12]</sup> Our study is based on a cathode made by carbon Super P with 30% of NiOCoO as catalyst in the presence and absence of O<sub>2</sub>. Actually, both cathodes (with and without O<sub>2</sub>) show the same impedance spectra from 4.0 to 2.7 V, in which extended electrochemical double layer capacitance (EDLC) made up by adsorbed Li<sup>+</sup> is observed. This capacitance has been verified on different systems and tested that is dependent on the surface area of the cathode. At lower voltages, the electrode in the presence of O<sub>2</sub> shows a huge capacitance increase at the same time that the EDLC is reduced. This fact evidences the depletion of the adsorbed Li<sup>+</sup> during the ORR. The results show three steps with their characteristic reaction time and resistance in the Li-O<sub>2</sub> discharge: (i) interfacial phenomena, (ii) EDLC, and (iii) chemical capacitance generated by oxygen reduction reaction (ORR capacitance). This study gives new insights onto the Li-O<sub>2</sub> discharge mechanism provided by impedance spectra, and highlights the key contribution on the overall ORR of adsorbed Li<sup>+</sup> on the electrode surface.

## 2. Results and Discussion

### 2.1. Electrochemical Behavior in the Presence and Absence of O<sub>2</sub>

Figure 1a shows the cyclic voltammetry (CV) of SP@30%NiOCoO in the presence of O<sub>2</sub> during cycling and in absence of O<sub>2</sub> (third cycle). Without O<sub>2</sub>, the CV signal shows some hysteresis (in the order of few mA g<sup>-1</sup>) without any remarkable peak (inset of Figure 1a). This shape is characteristic of supercapacitors in which the hysteresis is attributed to the EDLC built by the adsorption of Li<sup>+</sup> ions onto the carbon surface.<sup>[13]</sup> In the present case, the hysteresis is low because the

**Table 1.** Molecular percentage of Li in the form of Li<sub>2</sub>O<sub>2</sub> and Li<sub>2</sub>CO<sub>3</sub> determined by XPS (all data shown in the Supporting Information) in the sample cycles three, five or seven times at different stop voltage: 2.4 and 3.4 V.

| Sample          | Species [% mol]                      |                                       |
|-----------------|--------------------------------------|---------------------------------------|
|                 | Li (Li <sub>2</sub> O <sub>2</sub> ) | Li (Li <sub>2</sub> CO <sub>3</sub> ) |
| 3 cycles, 2.4 V | 3.6                                  | 1.4                                   |
| 3 cycles, 3.4 V | 0.3                                  | 0.6                                   |
| 5 cycles, 3.4 V | 5.6                                  | 11.2                                  |
| 7 cycles, 3.4 V | 6.9                                  | 19.4                                  |

surface area of the carbon matrix is small ( $S_{\text{BET}} = 75 \text{ m}^2 \text{ g}^{-1}$ ) compared to the carbon materials used for supercapacitors. The CV changes drastically in the presence of O<sub>2</sub>, where a cathodic peak is observed with an onset at 2.9 V and the maximum at 2.4 V, with the typical shape reported in the literature.<sup>[4,14]</sup> The shift of ORR peak from 2.7 to 2.4 V has been attributed to the EC mechanism, that is, electrochemical reduction (O<sub>2</sub> + e<sup>-</sup> → O<sub>2</sub><sup>-</sup>) followed by a chemical step (reaction of Li<sup>+</sup> with O<sub>2</sub><sup>-</sup>) that severely depletes the concentration of O<sub>2</sub><sup>-</sup>.<sup>[4]</sup> With the number of cycles, the cathodic peak reduces conspicuously, and in rather less extension the anodic peak. For this air cathode (of low  $S_{\text{BET}}$ ), the capacity is ≈500 mAh g<sup>-1</sup> (Figure SI.1, Supporting Information). The main species formed in the discharge process is Li<sub>2</sub>O<sub>2</sub>, which is almost decomposed during charge process, as revealed the XPS spectra (Figure SI.2, Supporting Information) that provides molecular percentage of Li in the form of Li<sub>2</sub>O<sub>2</sub> at 2.4 and 3.4 V after 3, 5, and 7 cycles (Table 1). XPS also shows that, in this case, Li<sub>2</sub>CO<sub>3</sub> is formed once Li<sub>2</sub>O<sub>2</sub> (very oxidative species that can react with the C of the electrode and/or the electrolyte) is produced,<sup>[6,15]</sup> albeit in little amount. Nevertheless, the decomposition of this residue is low and while Li<sub>2</sub>O<sub>2</sub> almost disappears during charge process, the residue reduces nearly a half. The evolution of the electrode composition is observed by XPS, where we could observe that Li<sub>2</sub>CO<sub>3</sub> is accumulated, as also pointed out by XRD (Figure 1b). Before cycling, the electrode shows the peaks ascribed to the mesh substrate and the catalyst, NiOCoO, the same result than the electrode at 3.4 V (before reduction process) after being cycled three times. Nevertheless, the characteristic peaks of Li<sub>2</sub>O<sub>2</sub> are observed after 5 CV, peaks that disappear after 7 cycles, where the characteristic Li<sub>2</sub>CO<sub>3</sub> peaks are clearly observed.

In order to assay the electrode in a representative state during Li-O<sub>2</sub> charge-discharge process, the electrochemical impedance spectroscopy was performed after three CV. The first cycle is discarded because it is not representative of a steady operation, and at the third cycle residual compounds are negligible, as XPS (Table 1 and Figure SI.2, Supporting Information) and XRD (Figure 1b) data demonstrate. The EIS measurements were carried out potentiostatically at different stages of Li<sup>+</sup> ion insertion at a very low rate to ensure the steady-state condition. Figure 2 shows three different Nyquist diagrams, representative of the different stages during the discharge process. The low frequencies range of the impedance spectra (below 5 Hz, indicated in Figure 2a,b) of both systems give the same Nyquist plot from ≈3.6 to 2.8 V. At 4.0 V (Figure 2a), the system with O<sub>2</sub> shows lower resistive behavior probably due to the degradation of the

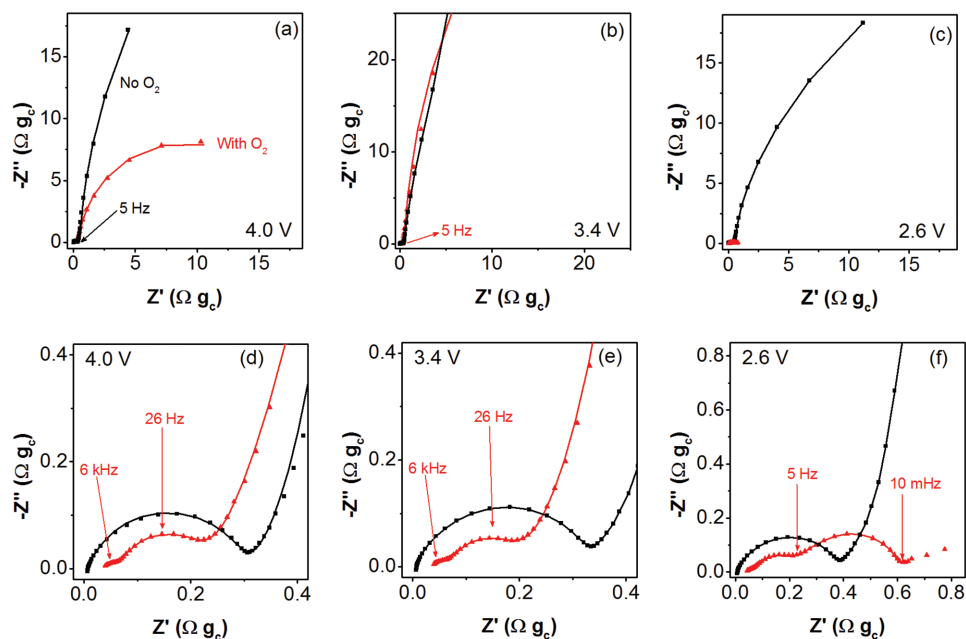


**Figure 2.** Nyquist plots of SP@30%NiOCoO with and without O<sub>2</sub>. The low frequency (<5 Hz) region of the EIS is observed in graphs a–c) and the figures d–f) show an enlargement of the high frequency region. The experimental data are represented by solid symbols and the lines are obtained by the fitting with the equivalent circuit model shown in Figure 4 b).

carbon cathode and the electrolyte solvent in the presence of O<sub>2</sub>, since carbon becomes unstable at voltages above 3.5 V.<sup>[16]</sup> At 2.6 V (and lower voltages), the Nyquist plot of the cathode in presence of O<sub>2</sub> changes drastically and the arc associated to the low frequency decreases dramatically. A new electrochemical feature is now observed at frequencies lower than 10 mHz (Figure 2f). This process should be related to the limiting step for ORR and O<sub>2</sub> diffusion. At high frequencies (above 5 Hz, Figure 2d–f), the Nyquist plots of the battery in absence of O<sub>2</sub> show one arc while there are two smaller arcs in the presence of O<sub>2</sub>.

To gain deeper insight on the Li-O<sub>2</sub> discharge kinetics, the impedance data are represented in terms of capacitance ( $C = 1/i\omega Z$ ) in Figure 3. In this representation, the real part,  $C'$ , is related to the electrode charging while the associated resistance caused by kinetic limitations determines the value reached by the imaginary part,  $C''$ . As explained elsewhere,<sup>[17]</sup> capacitive representation allows straightforwardly extracting contributing capacitors and, consequently, inferring on charging mechanisms.

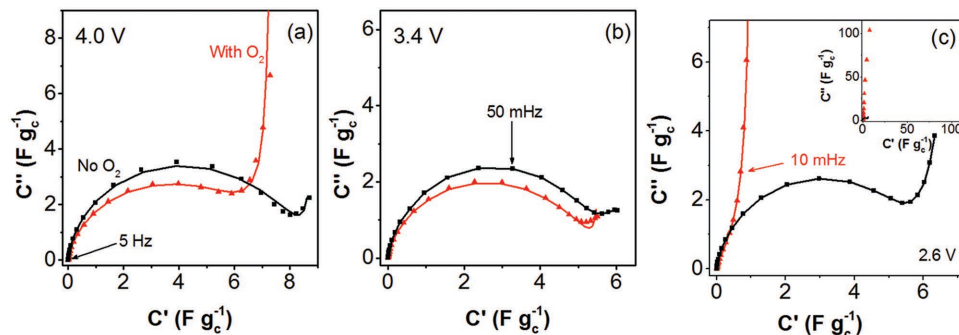


**Figure 3.** Capacitance plot of SP@30% NiOCoO with and without O<sub>2</sub>. The experimental data are represented by solid symbols and the lines are obtained by the fitting with the equivalent circuit model shown in Figure 4b).

Each arc in a capacitance plot is assimilated to a RC series sub-circuit. In the region of low frequencies (below 5 Hz) an arc is observed that closes to  $\approx 6.5 \text{ F g}_c^{-1}$  in the two systems (with and without O<sub>2</sub>) within the voltage range 4.0–2.8 V. At lower voltages, a new arc is observed in the presence of O<sub>2</sub> that is more than two orders of magnitude higher than the previous one, and hides it. At high frequencies (see Figure SI.3, Supporting Information), smaller arcs linked to different capacitive features in the multi-step discharge process are observed for both systems, although the capacitance in presence of O<sub>2</sub> is larger than in its absence.

## 2.2. Electrode Mechanisms Through Equivalent Circuits

Figure 4a represents the capacitance spectra,  $C'$ , versus characteristic time (inverse of measuring frequency) of the SP@30%NiOCoO cathode in the presence (solid lines) and absence (dashed lines) of O<sub>2</sub>. The horizontal axis is also represented in frequency scale, inversely than usually drawn, from

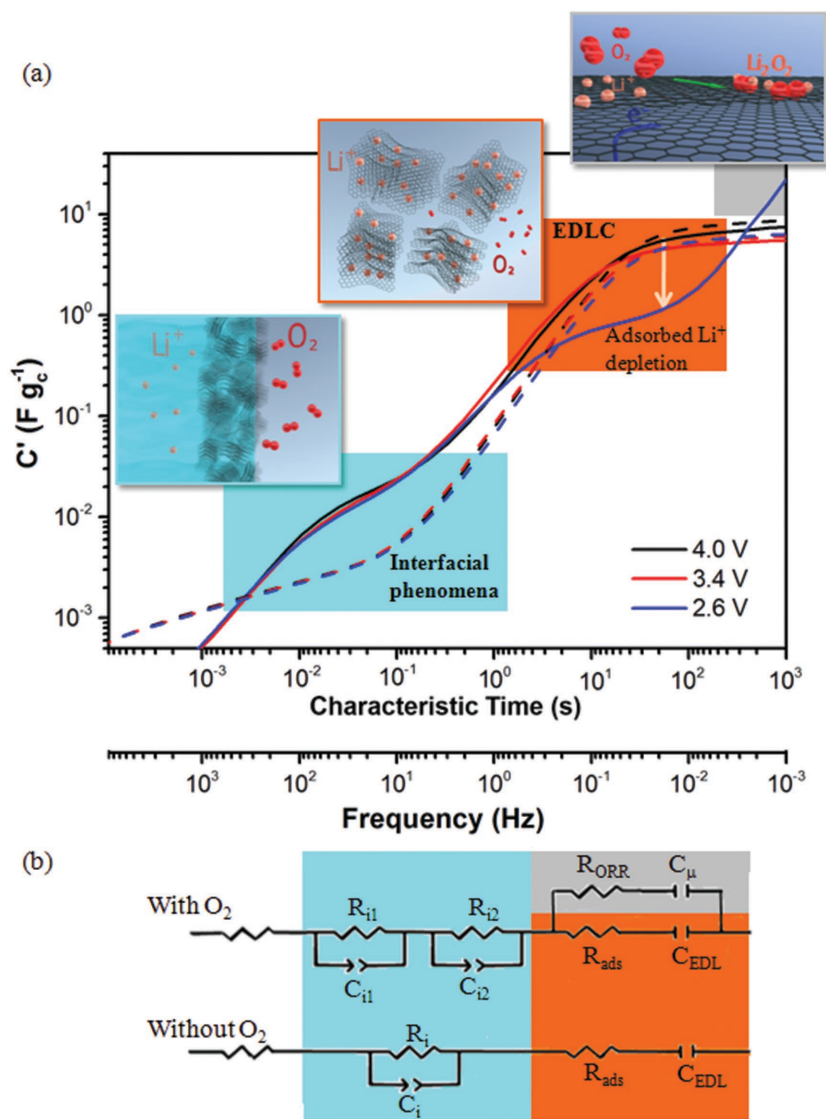


**Figure 4.** a)  $C'$  versus characteristic time and frequency (in opposite order than usual, from fast to slow electrochemical processes for a more intuitive reading) for SP@30%NiOCoO in the presence (solid lines) and absence (dashed lines) of  $O_2$ . Inset: Scheme of the three processes of the Li– $O_2$  discharge mechanism. The ORR is represented on the cathode surface by a graphitic layer, in which adsorbed  $Li^+$  react with  $O_2$ . b) Equivalent circuit model for the system in the absence and presence of  $O_2$ .

high to low frequency in order to maintain the same reading direction of the equivalent circuit model. In this representation, a plateau is demonstrative of a capacitive step in the discharge mechanism occurring at a certain frequency range. For electrodes with and without  $O_2$ , two plateaus are observed: the first one at intermediate frequencies ( $\approx 100$  Hz) is  $O_2$  dependent, while the second at low frequencies ( $\approx 0.01$  Hz) is  $O_2$  independent only at higher potentials. These two plateaus correspond to the two arcs described in Figure 3 and Figure SI.3, Supporting Information. The plateau at low frequencies is unaltered by the presence of  $O_2$  in all the discharge process until 2.6 V. Noticeably below this potential the presence of  $O_2$  induces the capacitance decreasing by one order of magnitude

showing a plateau that ends at 10 mHz. At lower frequencies the capacitance further increases in relation to the diffusion and reaction process discussed in Figure 2f.

By observing Figure 4a one can distinguish three steps in the discharge process, which are marked with squares and represented in the different subcircuits of the equivalent circuit model shown in Figure 4b. The fitting of the proposed equivalent circuit model is represented in Figures 2 and 3 with solid lines. The observed steps during discharge are:

- (i) Interfacial phenomena (high frequency:  $>5$  Hz) that is  $O_2$  dependent. In the presence of  $O_2$  two arcs are observed in the Nyquist plot, which are represented by two resistances ( $R_{i1}$  and  $R_{i2}$ ) in parallel with two capacitances ( $C_{i1}$  and  $C_{i2}$ ). In the absence of  $O_2$ , only one arc is observed that is equivalent to a resistance ( $R_i$ ) in parallel to the capacitance ( $C_i$ ).
- (ii) EDLC (intermediate frequency:  $10$  mHz  $< f < 5$  Hz) that is  $O_2$  independent at high potentials. This mechanism is connected to the  $Li^+$  adsorption on the internal electrode surface. This capacitance,  $C_{EDL}$ , is associated to an arc in the  $C''$  versus  $C'$  representation that can be modeled by a series RC circuit.<sup>[17,18]</sup> The associated resistance  $R_{ads}$  accounts for the  $Li^+$  transport in the electrolyte within the porous matrix. More details of this subcircuit model are in the Supporting Information.
- (iii) Chemical ORR capacitance (low frequency:  $<10$  mHz) that only appears in the presence of  $O_2$ . When  $O_2$  starts to react (at 2.8 V and below) a new parallel branch to the EDLC is represented in the equivalent circuit model by the chemical capacitance,  $C_{iU}$ , in series to the associated resistance,  $R_{ORR}$ , accounting for the reduction reaction.

### 2.3. Interfacial Phenomena

The electrochemical processes related to the interface are monitored by EIS at high frequencies. In the absence of  $O_2$ , a single semicircle is observed in the Nyquist representation (Figure 2 d–f) that is associated with a semicircle to the  $C''$  versus  $C'$  representation, Figure SI3, Supporting Information. This capacitance,  $C_i$ , and resistance,  $R_i$ , can be associated to the impedance generated at the contact interface between the electrode and the electrolyte solution.<sup>[19]</sup> In the presence of  $O_2$ , two small arcs are distinguished in Figure 2 d–f. One of the arcs can be ascribed to the formation of the insulating layer made up of  $Li_2O_2$  and  $Li_2CO_3$  (as XPS and XRD shown), and

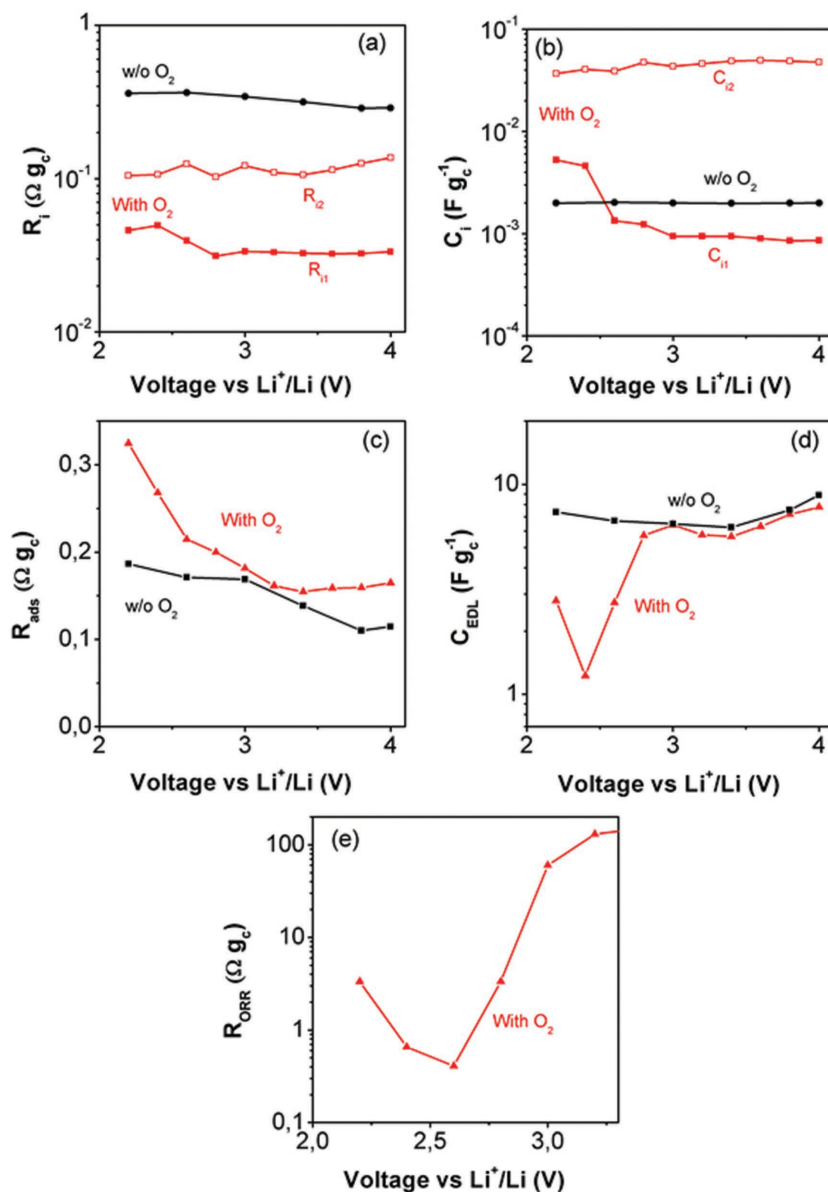


**Figure 5.** Parameters determined during discharge process by the EIS fitting with the equivalent circuit model shown in Figure 4b: a) resistance and b) capacitance associated to the interface phenomena; c) resistance,  $R_{\text{ads}}$ , and d) capacitance,  $C_{\text{EDL}}$ , associated to the formation of the electrochemical double layer; e) parallel resistance,  $R_{\text{ORR}}$ , which decrease at the applied voltages when the ORR starts.

the other to the impedance at the contact interface, as it has been assigned in the absence of O<sub>2</sub>. In any case these resistive elements introduce limitations into the overall charging mechanism.

The fitting values obtained by the equivalent circuit model are represented in Figure 5. With the calculated values, we can indicate that  $C_{12}$  and  $R_{12}$  are related to the electrode/electrolyte contact since they are constant independently of the applied voltage. In this assumption,  $C_{11}$  and  $R_{11}$  should be related to the solid electrolyte interface (Li<sub>2</sub>O<sub>2</sub> and Li<sub>2</sub>CO<sub>3</sub>) formed on the cathode, which explains why the capacitance increases with the oxygen reduction reaction.

#### 2.4. Electrochemical Double Layer Capacitance

With the equivalent circuit model (Figure 4b), the main parameters of the Li<sup>+</sup> adsorption step in the discharge process are obtained, Figure 5. In the absence of O<sub>2</sub>, the capacity is practically constant, 6.5  $\text{F g}_c^{-1}$  (that corresponds to  $\approx 8 \mu\text{F cm}_c^{-2}$  considering an area  $S_{\text{BET}} = 75 \text{ m}^2 \text{ g}_c^{-1}$ ), independently of the voltage. This value is within the range of reported electrochemical double layer capacitances in supercapacitors based on carbon materials (5–20  $\mu\text{F cm}_c^{-2}$ ).<sup>[13a]</sup> In this case, the capacitance is in agreement with a lower value obtained with supercapacitors when an organic electrolyte is used compared to aqueous electrolytes.<sup>[20]</sup> Associated to the charge accumulation by physical electroadsorption there is a resistance that has been related to the ion transport along the tortuous path of the micro/mesoporosity of the carbon matrix.<sup>[21]</sup> In the presence of O<sub>2</sub>, the EDL capacitance is unaltered at high voltages and noticeably decreases when the ORR starts. This is in accordance with recent capacitance analyses.<sup>[12]</sup> The resistance of the Li<sup>+</sup> adsorption process consistently increases, showing the kinetic competition between Li<sup>+</sup> adsorption and consumption by ORR at voltages lower than 2.8 V. At the same time, the parallel resistance,  $R_{\text{ORR}}$ , decreases dramatically (close to three orders of magnitude) giving further support to the idea that the current runs along the parallel branch corresponding to the ORR subcircuit in Figure 4b. At lower voltages than ORR reaction, (i.e., 2.2 V), the capacitance of the EDL starts to increase again signaling a full recovering of the double layer features. We infer that the ORR branch in Figure 4b is kinetically favored at potentials 2.4–2.8 V.

To check the role of species involved in the EDLC formation as a step in the discharge mechanism, other systems have been measured for consistency. The same results have been obtained in the absence of catalyst

(Figure SI.4, Supporting Information) and the study with carbons of different  $S_{\text{BET}}$  has revealed that EDLC can be considered only dependent on the carbon surface area (Figure SI.5, Supporting Information). This point is further discussed in the Supporting Information since depending on the size of the pores the area can be active or not to the formation of the EDL like in the case of supercapacitors.

In order to analyze the effect of cycling on the formation of the electric double layer, the electrochemical impedance spectrum at 3.4 V (during lithiation process) has been registered along several CV cycles. The Nyquist and capacitance plots are represented in Figure 6 and the obtained fitting parameters in

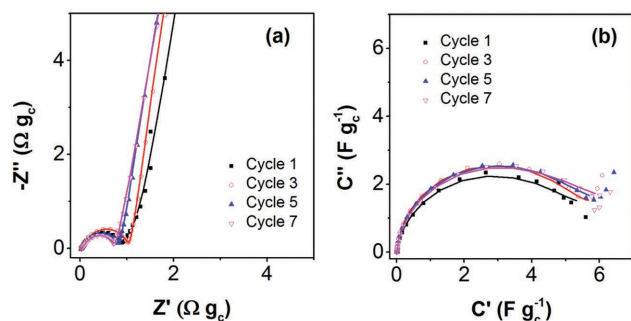


**Figure 6.** a) Nyquist and b) Capacitance plots of the SP@30%NiOCoO air cathode at 3.4 V at different number of CV cycles.

Figure S1.6, Supporting Information. Surprisingly, no significant differences are observed in the Nyquist plots, being the EDL capacitances practically constant, independently of the cycling number. This result shows that the electrode textural property is not modified after cycling, and  $\text{Li}^+$  cations can freely adsorb in the carbon internal surface, independently on the formation of  $\text{Li}_2\text{O}_2$  and  $\text{Li}_2\text{CO}_3$ , whose presence is evidenced by XPS and XRD.

With all the data in mind, the fact that EDL capacitance decreases when ORR starts due to a hiding phenomenon can be discarded since the EDL capacitance remains unaltered after cycling. If the reaction products (mainly  $\text{Li}_2\text{O}_2$ ) partially cover the carbon surface one would expect a reduction of the EDLC with cycling that does not occur at 3.4 V (Figure 6b). Therefore, the EDLC decrease with ORR should be associated to  $\text{Li}^+$  desorption, which can be either caused by: (i) displacement of physisorbed  $\text{Li}^+$  by chemisorbed  $\text{O}_2^-$  when ORR starts, followed by the subsequent chemical reaction between adsorbed  $\text{O}_2^-$  with the solved  $\text{Li}^+$  in the electrolyte or (ii) to a direct reaction between the physisorbed  $\text{Li}^+$  with the molecular  $\text{O}_2$  at the oxygen reduction potential to give  $\text{Li}_2\text{O}_2$ . Nevertheless, once the potential of ORR is surpassed (i.e., 2.2 V), the EDL capacitance increases again, what suggests that  $\text{Li}_2\text{O}_2$  is not forming a monolayer on the top of the carbon surface. This idea is also supported by the study of  $C_{\text{EDL}}$  with the number of cycles, in which is observed that the same capacitance is obtained independently on the number of CV cycles, and then, on the formation of  $\text{Li}_2\text{O}_2$  and  $\text{Li}_2\text{CO}_3$ . This result discards that the transport limitation and the cause of the low rechargeability of the current battery is the formation of an insulating layer ( $\text{Li}_2\text{CO}_3$  or  $\text{Li}_2\text{O}_2$ ) on the carbon internal surface, as some authors have reported.<sup>[6,22]</sup> Therefore, the transport blocking most probably become from the accumulation of these two species on one of the two sides of the electrode (electrode–electrolyte or electrode– $\text{O}_2$ ). Since the surface phenomena monitored by EIS (related to the electrode–electrolyte interface) are scarcely affected by the presence of these two species, one can infer that the accumulation of both,  $\text{Li}_2\text{O}_2$  and  $\text{Li}_2\text{CO}_3$ , is at the electrode– $\text{O}_2$  interface, that finally limits the  $\text{O}_2$  diffusion.<sup>[23]</sup> Noticeably EDLC remains unaltered after cycling. This fact suggests that the ORR products ( $\text{Li}_2\text{O}_2$  and  $\text{Li}_2\text{CO}_3$ ) are not covering the internal electrode surface, but deposited on the outer electrode– $\text{O}_2$  interface, hindering thereby the subsequent reaction.

In all the models for  $\text{Li}-\text{O}_2$  discharge mechanism, the surface of the cathode is considered as a raw graphitic layer where

the  $\text{Li}^+$  ions arrive from the electrolyte side. This study demonstrates that the surface is already covered by adsorbed  $\text{Li}^+$  when ORR starts, what it could imply that for the soluble  $\text{O}_2$  to react with  $\text{Li}^+$ , the molecular  $\text{O}_2$  can first react with the adsorbed  $\text{Li}^+$  on the surface nearly the outer  $\text{O}_2$  entrance layer, forming  $\text{Li}_2\text{O}_2$  and avoiding further reaction. Qu and co-workers<sup>[11]</sup> reported that the discharge capacitance can be increased with  $\text{O}_2$  pressure higher than 1 atm since the electrolyte was forced back from the interface and the complete wetting of the cathode is avoided. Therefore, adsorbed  $\text{Li}^+$  consumption provides a new context of the cathode surface where the oxygen reduction reaction develops.

## 2.5. ORR Capacitance

At low voltages the reduction reaction of  $\text{O}_2$  takes place. ORR is the main process in  $\text{Li}-\text{O}_2$  batteries that provides the unique high capacity, but the main drawback for following this reaction by EIS is its extremely slow rate; it is registered at frequencies below 10 mHz. For this reason, the fitting of the data is only partial. In Figure 4b it has been represented by a resistance in series with the chemical capacitance for the purpose of clarity. Nevertheless, in the Nyquist plot is observed that the real part of the impedance ( $-Z'$ ) increases, then signaling an extra resistive behavior in addition to the capacitive one observed in Figure 4a. For this reason, more elements than the chemical capacitance are certainly needed. It is indeed the final limiting step related to the  $\text{O}_2$  diffusion through different layers. It is obvious that it is necessary to fast up this process in order to make it fully observable by impedance methods.

## 3. Experimental Section

All the agents were purchased from Sigma Aldrich, and were used as received. The cathodes were prepared by painting a carbon/PVdF slurry onto a stainless steel mesh. The slurries were prepared by mixing carbon black/PVdF/catalyst (60:10:30% wt) and the addition of 1-methyl-2-pyrrolidone. All the cathodes were dried in vacuum, at 110 °C overnight. Mixed-metal oxides are proved to be good catalysts for both ORR and OER in  $\text{Li}-\text{O}_2$  batteries.<sup>[24]</sup> In this study, a commercial nanopowder, nickel cobalt oxide, (of size lower than 150 nm, CAS 5859–45–0, Sigma-Aldrich) was observed to accelerate  $\text{H}_2\text{O}_2$  oxidation (Figure S1.8, Supporting Information) and, consequently, it is a good candidate as catalyst for  $\text{Li}-\text{O}_2$  batteries,<sup>[25]</sup> albeit no reference of its use has been found in the literature. Despite its study is out of the topic of this article, we have seen that its main contribution is the reduction of the charge transfer resistance (Figure S1.9, Supporting Information).

Cell assembly (Swagelok type) was carried out in a  $\text{N}_2$  filled glovebox. This consists simple in clamping together a Li metal foil anode, an electrolyte-soaked separator, the electrolyte that is 1 M hexafluorophosphate lithium salt ( $\text{LiPF}_6$ ) dissolved in tetraethylene glycol dimethyl ether (TEGDME), the cathode under study and the stainless steel current collector. The cathode collector is a tube in which pure  $\text{O}_2$  (>99.9999 to avoid contamination issues) flows, the pressure is maintained at 1 atm during all the experiment.

Electrochemical characterization was performed using a PGSTAT30 potentiostat from Autolab equipped with an impedance module. The CV was carried out in the voltage window of 2–4.0 V at 100  $\mu\text{V s}^{-1}$  scan rate. After 3 CV scans, the EIS spectra were performed (every 200 mV) within

this voltage range with an amplitude perturbation of 10 mV, and in the frequency range of 1 MHz to 1 mHz. The approximation to the different voltages of measurement was potentiostatically controlled at  $10 \mu\text{V s}^{-1}$  to assure the quasi-equilibrium state of the battery. Also, before each measurement the system was stabilized during 30 min. All the data are normalized to the carbon mass.

The cycled electrodes were characterized by means of X-ray powder diffraction (XRD) using Bruker AXS-D4 Endeavor Advance X-ray diffractometer using  $\text{Cu}_\alpha$  radiation. X-ray photoelectron spectroscopy (XPS) was performed on Sage 150 de Specs with non-monochromatic radiation  $\text{AlK}\alpha$  (1486.6 eV) to 20 mA and 13 kV, a constant pass energy 75 eV for global analysis and 30 eV for specific binding energy of each element analysis, and an area measuring  $1 \times 1 \text{ mm}^2$ . The base pressure of XPS chamber was  $7 \times 10^{-9}$  hPa. XPS spectra were fitted with CasaXPS software, which models the Gauss–Lorentzian contributions, after background subtraction. Also, energy spectra were calibrated by setting the C 1s photoemission peak for  $\text{sp}^2$ -hybridized carbon to 284.8 eV. Samples were washed out by anhydrous dimethyl carbonate (DMC, Sigma-Aldrich) solvent several times, and dried in a vacuum chamber at  $60^\circ\text{C}$  for 2 h previous XRD and XPS measurements.<sup>[26]</sup>

## 4. Conclusions

This article analyzes the discharge process of  $\text{Li-O}_2$  batteries by impedance spectroscopy and provides a novel equivalent circuit model. In this model, different electrochemical processes during discharge mechanism are identified: (i) interfacial phenomena, (ii) EDLC, and (iii) ORR chemical capacitance. EDLC has been monitored in  $\text{Li-O}_2$  batteries and it is observed to be independent of the presence of  $\text{O}_2$  at voltages higher than those at which oxygen reduction reaction occurs. Noticeably EDLC is fully recovered after electrode charging, and remains unaltered after cycling. This fact suggests that the ORR products ( $\text{Li}_2\text{O}_2$  and  $\text{Li}_2\text{CO}_3$ ) are not covering the internal electrode surface, but deposited on the outer electrode- $\text{O}_2$  interface, hindering thereby the subsequent reaction. At this moment, further research is necessary to elucidate if these adsorbed  $\text{Li}^+$  at the internal electrode double layer can directly react with the  $\text{O}_2$  molecules at the voltage where ORR starts or they are merely displaced by the reduction of  $\text{O}_2$  molecules. The novel equivalent circuit model and the consideration that  $\text{Li}^+$  ions are already adsorbed on the carbon surface when ORR starts provide new tools in the study and design of  $\text{Li-O}_2$  cathodes.

## Supporting Information

Supporting Information is available from the Wiley Online Library or from the author.

## Acknowledgements

The authors thank financial support from Generalitat Valenciana (ISIC/2012/008 Institute of Nanotechnologies for Clean Energies). The authors acknowledge Dr. Conchi Ania from National Institute of Carbon for providing PSCo and AG carbons and their characterization.

Received: July 9, 2015

Published online:

- [1] P. G. Bruce, S. A. Freunberger, L. J. Hardwick, J.-M. Tarascon, *Nat. Mater.* **2012**, *11*, 19.
- [2] N. S. Choi, Z. Chen, S. A. Freunberger, X. Ji, Y. K. Sun, K. Amine, G. Yushin, L. F. Nazar, J. Cho, P. G. Bruce, *Angew. Chem. Int. Ed.* **2012**, *51*, 9994.
- [3] a) Z. Peng, S. A. Freunberger, Y. Chen, P. G. Bruce, *Science* **2012**, *337*, 563; b) H.-G. Jung, J. Hassoun, J.-B. Park, Y.-K. Sun, B. Scrosati, *Nat. Chem.* **2012**, *4*, 579; c) B. G. Kim, H.-J. Kim, S. Back, K. W. Nam, Y. Jung, Y.-K. Han, J. W. Choi, *Sci. Rep.* **2014**, *4*, d) Z. L. Wang, D. Xu, J. J. Xu, L. L. Zhang, X. B. Zhang, *Adv. Funct. Mater.* **2012**, *22*, 3699.
- [4] Z. Peng, S. A. Freunberger, L. J. Hardwick, Y. Chen, V. Giordani, F. Bardé, P. Novák, D. Graham, J. M. Tarascon, P. G. Bruce, *Angew. Chem.* **2011**, *123*, 6475.
- [5] R. Wen, M. Hong, H. R. Byon, *J. Am. Chem. Soc.* **2013**, *135*, 10870.
- [6] B. McCloskey, A. Speidel, R. Scheffler, D. Miller, V. Viswanathan, J. Hummelshøj, J. Nørskov, A. Luntz, *J. Phys. Chem. Lett.* **2012**, *3*, 997.
- [7] B. Scrosati, K. M. Abraham, W. A. van Schalkwijk, J. Hassoun, *Lithium Batteries: Advanced Technologies and Applications*, Wiley, Hoboken, New Jersey, **2013**.
- [8] C. O. Laoire, S. Mukerjee, K. Abraham, E. J. Plichta, M. A. Hendrickson, *J. Phys. Chem. C* **2009**, *113*, 20127.
- [9] a) M. D. Radin, D. J. Siegel, *Energy Environ. Sci.* **2013**, *6*, 2370; b) C. O. Laoire, S. Mukerjee, K. Abraham, E. J. Plichta, M. A. Hendrickson, *J. Phys. Chem. C* **2010**, *114*, 9178; c) M. Safari, B. D. Adams, L. F. Nazar, *J. Phys. Chem. Lett.* **2014**, *5*, 3486; d) B. Horstmann, B. Gallant, R. Mitchell, W. G. Bessler, Y. Shao-Horn, M. Z. Bazant, *J. Phys. Chem. Lett.* **2013**, *4*, 4217; e) J.-J. Xu, Z.-L. Wang, D. Xu, L.-L. Zhang, X.-B. Zhang, *Nat. Commun.* **2013**, *4*, 2438.
- [10] a) L. Johnson, C. Li, Z. Liu, Y. Chen, S. A. Freunberger, P. C. Ashok, B. B. Praveen, K. Dholakia, J.-M. Tarascon, P. G. Bruce, *Nat. Chem.* **2014**, *6*, 1091; b) K.-H. Xue, E. McTurk, L. Johnson, P. G. Bruce, A. A. Franco, *J. Electrochem. Soc.* **2015**, *162*, A614.
- [11] C. Tran, X.-Q. Yang, D. Qu, *J. Power Sources* **2010**, *195*, 2057.
- [12] J. Højberg, B. D. McCloskey, J. Hjelm, T. Vegge, K. Johansen, P. Norby, A. C. Luntz, *ACS Appl. Mater. Interfaces* **2015**, *7*, 4039.
- [13] a) P. Simon, Y. Gogotsi, *Nat. Mater.* **2008**, *7*, 845; b) M. Haro, G. Rasines, C. Macias, C. Ania, *Carbon* **2011**, *49*, 3723.
- [14] a) S. Y. Kim, H.-T. Lee, K.-B. Kim, *Phys. Chem. Chem. Phys.* **2013**, *15*, 20262; b) F. Li, R. Ohnishi, Y. Yamada, J. Kubota, K. Domen, A. Yamada, H. Zhou, *Chem. Commun.* **2013**, *49*, 1175.
- [15] S. A. Freunberger, Y. Chen, N. E. Drewett, L. J. Hardwick, F. Bardé, P. G. Bruce, *Angew. Chem. Int. Ed.* **2011**, *50*, 8609.
- [16] M. M. Ottakam Thotiyl, S. A. Freunberger, Z. Peng, P. G. Bruce, *J. Am. Chem. Soc.* **2012**, *135*, 494.
- [17] F. Martinez-Julian, A. Guerrero, M. Haro, J. Bisquert, D. Bresser, E. Paillard, S. Passerini, G. Garcia-Belmonte, *J. Phys. Chem. C* **2014**, *118*, 6069.
- [18] M. Haro, T. Song, A. Guerrero, L. Bertoluzzi, J. Bisquert, U. Paik, G. Garcia-Belmonte, *Phys. Chem. Chem. Phys.* **2014**, *16*, 17930.
- [19] W.-C. Chen, T.-C. Wen, *J. Power Sources* **2003**, *117*, 273.
- [20] C. Vix-Guterl, S. Saadallah, K. Jurewicz, E. Frackowiak, M. Reda, J. Parmentier, J. Patarin, F. Beguin, *Mater. Sci. Eng.: B* **2004**, *108*, 148.
- [21] F. Béguin, E. Frackowiak, *Carbons for Electrochemical Energy Storage and Conversion Systems*, CRC Press, Boca Raton, Florida, **2009**.
- [22] P. Albertus, G. Girishkumar, B. McCloskey, R. S. Sánchez-Carrera, B. Kozinsky, J. Christensen, A. Luntz, *J. Electrochem. Soc.* **2011**, *158*, A343.
- [23] S. Sandhu, J. Fellner, G. Brutchén, *J. Power Sources* **2007**, *164*, 365.

- [24] a) J.-J. Xu, Z.-L. Wang, D. Xu, F.-Z. Meng, X.-B. Zhang, *Energy Environ. Sci.* **2014**, *7*, 2213; b) J. J. Xu, D. Xu, Z. L. Wang, H. G. Wang, L. L. Zhang, X. B. Zhang, *Angew. Chem. Int. Ed.* **2013**, *52*, 3887.
- [25] V. Giordani, S. Freunberger, P. Bruce, J.-M. Tarascon, D. Larcher, *Electrochem. Solid-State Lett.* **2010**, *13*, A180.
- [26] M. H. Rui Wen, Hye Ryung Byon, *J. Am. Chem. Soc.* **2013**, *135*, 10870.
-